Ultrastructure of influenza virus ribonucleoprotein complexes during viral RNA synthesis

Masahiro Nakano
Kyoto University https://orcid.org/0000-0003-4247-9008
Yukihiko Sugita
Kyoto University https://orcid.org/0000-0001-6861-4840
Noriyuki Kodera
Kanazawa University
Sho Miyamoto
Kyoto University
Yukiko Muramoto
Kyoto University
Matthias Wolf
Okinawa Institute of Science and Technology Graduate University, Japan
Takeshi Noda (t-noda@infront.kyoto-u.ac.jp)
Kyoto University

Article

Keywords: influenza virus, viral RNA synthesis

Posted Date: February 16th, 2021

DOI: https://doi.org/10.21203/rs.3.rs-198950/v1

Version of Record: A version of this preprint was published at Communications Biology on October 27th, 2021. See the published version at https://doi.org/10.1038/s42003-021-02388-4.

Ultrastructure of influenza virus ribonucleoprotein complexes during viral RNA synthesis

Masahiro Nakano[1,2], Yukihiko Sugita[1,3,4], Noriyuki Kodera[5], Sho Miyamoto[1], Yukiko Muramoto[1,2], Matthias Wolf[4], and Takeshi Noda[1,2,6*]

[1]Laboratory of Ultrastructural Virology, Department of Virus Research, Institute for Frontier Life and Medical Sciences, Kyoto University, 53 Shogoin Kawahara-cho, Sakyo-ku, Kyoto 606-8507, Japan. [2]Graduate School of Biostudies, Kyoto University, 53 Shogoin Kawahara-cho, Sakyo-ku, Kyoto 606-8507, Japan. [3]Hakubi Center for Advanced Research, Kyoto University, Yoshida-honmachi, Sakyo-ku, Kyoto 606-8501, Japan. [4]Molecular Cryo-Electron Microscopy Unit, Okinawa Institute of Science and Technology Graduate University, 1919-1 Tancha, Onna-soen, Kunigami-gun, Okinawa 904-0495, Japan. [5]Nano Life Science Institute (WPI-NanoLSI), Kanazawa University, Kakuma, Kanazawa 920-1192, Japan. [6]PRESTO, Japan Science and Technology Agency, 4-1-8 Honcho, Kawaguchi, Saitama 332-0012, Japan.

*correspondence to: t-noda@infront.kyoto-u.ac.jp

The single-stranded, negative-sense, viral genomic RNA (vRNA) of influenza A virus is encapsidated by viral nucleoproteins and an RNA polymerase to form a ribonucleoprotein complex (vRNP) with a helical, rod-shaped structure. The vRNP is responsible for transcription and replication of the vRNA. However, the vRNP conformation during viral RNA synthesis is not well understood. Here, using high-speed atomic force microscopy and cryo-electron microscopy, we investigated the native structure of influenza A vRNPs during RNA synthesis *in vitro*. Two distinct types of vRNPs were observed in association with newly synthesized RNAs: an intact, helical rod-shaped vRNP connected with a structured viral RNA product and a deformed vRNP associated with a looped, double-stranded RNA, composed of a template vRNA and a nascent RNA. These results suggest that while some vRNPs keep their helical structures during viral RNA synthesis, probably for the repeated cycle of transcription and/or replication, others accidentally become structurally deformed, which probably results in failure to commence or continue RNA synthesis. Thus, our findings provide the ultrastructural basis of viral RNA synthesis and advance our knowledge of the mechanism of viral transcription and replication.

Influenza A virus, a member of the *Orthomyxoviridae,* has eight, single-stranded, negative-sense RNA segments (vRNAs) as its genome. Transcription and replication of influenza A virus are carried out by ribonucleoprotein complexes called vRNPs in the nucleus of infected cells. A vRNP consists of a vRNA, multiple copies of nucleoprotein (NP), and a heterotrimeric, RNA-dependent RNA polymerase complex comprising PB2, PB1, and PA subunits (1–4). Each vRNP adopts a helical, rod-shaped structure, in which an NP-vRNA strand is folded back on itself and coiled, forming a double-stranded helix with a loop structure at one end (5, 6). The heterotrimeric RNA polymerase is located opposite to the loop end of the helical rod-shaped vRNP (7–9).

Although influenza virus vRNPs conduct both transcription and replication of the vRNAs, mechanisms of the two processes are quite different. During transcription, the PB2 subunit binds to the 5'-terminal methylated cap structure (m^7GpppXm) of host pre-mRNAs (10, 11), and the PA subunit cleaves the pre-mRNA 10–13 nucleotides downstream from the cap with its endonuclease activity (12–14). The resultant capped RNA fragment is directed to the PB1 active site where it is used as a primer (15). After elongation, a poly(A) tail is added to the 3' end of the transcript by stuttering of the polymerase on the oligo-U stretch of the template vRNA (16–18). Hence, the 5'-capped and 3'-polyadenylated viral mRNAs are synthesized in a primer-dependent manner. In

53 contrast, genome replication is thought to be primer-independent (19). Replication
54 involves generation of positive-sense complementary RNAs (cRNAs), which are
55 replication intermediates that act as templates for vRNA synthesis. Elongation of a
56 nascent cRNA by *cis*-acting RNA polymerase proceeds concomitantly with sequential
57 binding of free NPs, forming a rod-shaped, double-helical cRNP complex (20–22).
58 Afterward, *trans*-acting or *trans*-activating RNA polymerase generates vRNAs from
59 intermediate cRNAs (21, 23, 24).

60 Great progress has been made in delineating the molecular mechanisms by which
61 the RNA polymerase conducts transcription and replication based on its atomic structure
62 (15, 18, 24–30). However, it is the vRNP rather than the RNA polymerase that
63 accomplishes viral genome transcription and replication. Recently, Coloma *et al.*
64 investigated the structure of the vRNP during *in vitro* transcription using cryo-electron
65 microscopy (cryo-EM) and concluded that the vRNPs maintain their double helical
66 structures during transcription (31). However, because nascent RNAs were barely visible
67 together with potentially transcribing vRNPs, it remains unclear whether the vRNPs
68 observed were producing nascent RNA. Here, to further characterise transcription and
69 replication from an ultrastructural perspective, we analysed virion-derived vRNPs
70 producing nascent viral RNAs during *in vitro* RNA synthesis, using high-speed atomic

71 force microscopy (HS-AFM) and cryo-EM. The combination of these two techniques
72 enabled us to clearly visualize and characterise the native structures of vRNPs producing
73 nascent viral RNAs.
74

Results

Virion-derived vRNPs produce both mRNA and cRNA *in vitro*

It has been reported that vRNPs isolated from influenza virions synthesize both mRNA and cRNA *in vitro* by adding ApG or globin mRNA as a primer (32). To investigate the structure of vRNP during transcription and replication, we purified vRNPs from influenza A virions and performed *in vitro* RNA synthesis using primers. Autoradiography of the RNA products after electrophoresis showed bands corresponding to the eight vRNAs of influenza A virus in a 15-min incubation after the reactions (Fig. 1a, Supplementary Fig. 1a, b). Treatment of an influenza virus RNA polymerase inhibitor, 6-fluoro-3-hydroxy-2-pyrazinecarboxamide-4-ribofuranosyl-5'-triphosphate (T-705RTP) (33), decreased the band intensity in a dose-dependent manner (Fig. 1b), confirming that viral RNAs are synthesized from virion-derived vRNPs.

Then, to determine whether vRNPs produce both cRNA and mRNA, we performed strand-specific reverse transcription-quantitative real-time polymerase chain reaction (RT-qPCR) for the NP and NA genes (34). Here, because 5' capped mRNA cannot be generated using ApG as a primer, we defined positive-strand viral RNA containing poly(A) tail at its 3' end as mRNA. Non-specific amplification was barely detectable (Supplementary Fig. 2a, b). In the absence of the primers, cRNA and mRNA were hardly

93 detected, except for NP mRNA (Supplementary Fig. 2c, d). Addition of either ApG or
94 globin mRNA primer resulted in production of 1×10^5–5×10^6 copies μL^{-1} of cRNA and
95 mRNA of both NP and NA segments (Supplementary Fig. 2c, d). These results
96 demonstrated that virion-derived vRNPs produce both cRNA and mRNA in the presence
97 of primers. Since there was no significant difference in the level of viral RNA production
98 between ApG-primed and globin mRNA-primed samples, we used ApG as a primer in
99 subsequent ultrastructural analysis.
100
101 **During viral RNA synthesis, vRNPs show two distinctive structures**
102 Although vRNPs are helical rod-shaped structures in a static state, it is possible that they
103 may change their conformations during viral RNA synthesis. To investigate near-native
104 vRNP structures producing nascent viral RNA, we employed HS-AFM, which can
105 provide topographic images in solution by scanning sample surfaces with a probe tip,
106 without fixation or staining (35). After *in vitro* RNA synthesis, vRNPs were adsorbed
107 onto a mica substrate and were visualized in solution. Without the primer, after *in vitro*
108 RNA synthesis, vRNPs appeared as rod-shaped structures with helical grooves (Fig. 1c),
109 which is typical of vRNP structures visualized by negative-staining EM (5). Immediately
110 after adding ApG primer (0 min), vRNPs maintained helical rod-shaped structures (Fig.

111 1d). However, after a 15-min incubation with ApG primer, vRNPs showed distinctive
112 structures that were associated with potentially nascent viral RNA. On the basis of their
113 configurations, we classified vRNP-RNA complexes into two groups: helical rod-shaped
114 vRNPs associated with a structured RNA (Fig. 1e, f, Supplementary Fig. 3), and deformed
115 vRNPs associated with a looped RNA (Fig. 1g, h). The configuration of vRNPs bound to
116 the structured RNA appeared similar to those of control vRNPs (Fig. 1c). Their diameters
117 were almost uniform and helical grooves could be observed along entire rod-shaped
118 vRNPs, suggesting no apparent conformational changes. Structured RNAs, which seem
119 to contain some secondary structures, were associated not only with the tip (Fig. 1e,
120 Supplementary Fig. 3a), but also with the bodies of helical rod-shaped vRNPs (Fig. 1f,
121 Supplementary Fig. 3b). By contrast, the configuration of vRNPs associated with looped
122 RNAs was substantially deformed, such that helical grooves of the vRNPs had
123 disappeared (Fig. 1g, h). vRNPs associated with looped RNA comprised 30.2% of all
124 vRNP-RNA complexes (N = 96).
125 To exclude the possibility that vRNPs became physically deformed after being
126 tapped with the AFM probe tip, we observed unstained frozen-hydrated samples of
127 vRNP-RNA complexes using cryo-EM. Both helical rod-shaped vRNPs associated with
128 structured RNA (Fig. 2a) and deformed vRNPs associated with looped RNA (Fig. 2b)

appeared similar to those observed with HS-AFM, suggesting that deformation of vRNPs occurs during RNA synthesis. To further investigate the configuration of vRNP-RNA complexes in more detail, we performed low-dose cryo-electron tomography (cryo-ET) to analyse their three-dimensional structure. A vRNP without *in vitro* RNA synthesis showed a double helical structure with several grooves (Fig. 2c), consistent with vRNPs reconstructed by single-particle cryo-EM (7, 8, 31). The tomographic reconstruction of a deformed vRNP was able to resolve the continuous RNA loop associated with the deformed vRNP (Fig. 2d), where both ends of the loop structure were located relatively close to each other on the deformed vRNP, suggesting that the viral RNA polymerase exists at the looped RNA-binding site, although its structure was not resolved. Interestingly, we found that the vRNP partially maintained a double helical structure at one end, and only the portion to which both ends of the looped RNA were bound was deformed (Fig. 2d), suggesting that deformation of the helical rod-shaped vRNP is likely participating in RNA synthesis. Unfortunately, the helical rod-shaped vRNP associated with a structured RNA could not be technically reconstructed, because RNAs with pleomorphic structure were not visible enough for cryo-ET due to low-contrast images of cryo-EM, as shown previously (31).

Both structured and looped RNAs associated with vRNPs are viral RNA products

Next, to determine whether the observed structured and looped RNAs are products synthesized by vRNPs, we used a nucleotide analogue, 5-bromo-UTP (Br-UTP), for *in vitro* RNA synthesis. When Br-UTP was used for *in vitro* RNA synthesis instead of UTP, both structured and looped RNAs associated with vRNPs were similarly observed (Fig. 3a, b, respectively). On incubation with the antibody, which reacts with Br-UTP present only in a single-strand RNA, specific binding of the antibody to the structured RNAs was observed (Fig. 3c, Supplementary Fig. 4), whereas the antibody did not react with structured RNAs produced by *in vitro* RNA synthesis using UTP (Fig. 3e), indicating that the structured RNAs are single-strand, nascent RNAs synthesized by the associated vRNPs. By contrast, the antibody did not bind to looped RNAs produced during *in vitro* RNA synthesis using Br-UTP (Fig. 3d) or UTP (Fig. 3f). Since the looped RNA has no secondary structure, we presumed that it might be double-stranded RNA (dsRNA). To test this hypothesis, RNase for digesting either single-stranded RNA (RNase A) or dsRNA (RNase III) was added to the looped RNAs and examined *in situ* using HS-AFM. With RNase A treatment, one end of the looped RNA was often detached from the vRNP and became straight, but the looped RNA itself was not digested, suggesting that it is double-stranded except at one end (Fig. 4a, Supplementary movie 1). In contrast, RNase III

digested looped RNAs (Fig. 4b, Supplementary movie 2). Upon binding, the RNase III molecule immediately digested the RNA, which was further shortened by sequential binding of more RNase III molecules, confirming that the looped RNA was dsRNA. This finding was further verified using anti-dsRNA antibody. The antibodies efficiently recognised the looped RNA associated with vRNPs (Fig. 4c, Supplementary movie 3), while only a few antibody molecules were bound to parts of the structured RNA, probably through stem-loop regions within the single-stranded RNA (Fig. 4d, Supplementary movie 4). Then, do influenza viruses generate dsRNA during the transcription and replication? To address this question, Vero cells were infected with PR8 virus and were subjected to immunofluorescence assay (IFA) by using anti-dsRNA antibody. At 10 h post infection, dsRNAs were detected in the nucleus of infected cells (Fig. 4e), but not in mock-infected cells, suggesting that influenza viruses produce dsRNA and that the deformed vRNP structures associating with the looped RNA may also be produced in the infected cells.

Next, to determine whether double-stranded, looped RNA contains nascent RNA, we used 5-ethynyl-UTP (EUTP) for *in vitro* RNA synthesis and evaluated its incorporation into looped RNAs using Click chemistry. A Click reaction with biotin-azide was followed by incubation with streptavidin, and specific binding of streptavidin to

183 looped RNAs was confirmed with HS-AFM (Fig. 3g). However, without streptavidin
184 (Supplementary Fig. 5a) or a Click reaction (Supplementary Fig. 5b), during *in vitro* RNA
185 synthesis using UTP as a substrate (Fig. 3h), binding of streptavidin to the looped RNAs
186 was not observed, suggesting that double-stranded, looped RNAs encompass nascent
187 viral RNAs produced by associated vRNPs. Taken together, these results indicate that
188 both structured and double-stranded looped RNAs associated with vRNPs are viral RNA
189 products formed during *in vitro* RNA synthesis.
190
191 **vRNA is partially dissociated from deformed vRNP associated with looped dsRNA**
192 Given that looped dsRNA contains a single-strand nascent viral RNA, it is likely that its
193 counterpart is the template vRNA dissociated from the deformed vRNP during RNA
194 synthesis. Hence, it is expected that deformed vRNPs have lower structural stability than
195 intact vRNPs due to loss of its vRNA as a structural component. To determine whether
196 deformed vRNPs lose the vRNA, at least in part, we examined the structural stability of
197 vRNPs by applying force with the cantilever tip during HS-AFM imaging (Fig. 5). Since
198 vRNAs within vRNPs are sensitive to RNase (36), vRNPs treated with a low
199 concentration of RNase A were prepared as control vRNPs that lacked intact residential
200 vRNA (Supplementary Fig. 6). Although vRNPs treated with RNase A maintained their

helical rod-shaped structures, they were easily broken with significantly less force (Fig. 5a, the bottommost panel) than those vRNPs untreated with RNase A (Fig. 5a, the uppermost panel). vRNPs associated with structured viral RNA were physically stable, much as intact vRNPs, whereas vRNPs associated with double-stranded, looped viral RNA were broken with significantly less force, as is the case with RNase A-treated vRNPs (Fig. 5a, b). Collectively, these results strongly suggest that at least some parts of template vRNA are detached from NPs of vRNP during RNA synthesis, resulting in formation of double-stranded, looped RNA with nascent viral RNA, and consequent deformation of helical rod-shaped vRNPs.

Discussion

vRNP is responsible for transcription and replication of the influenza virus genome. Thus far, details of its structure during viral RNA synthesis have been largely unknown due to technical limitations. Here, we employed HS-AFM and cryo-EM to visualise near-native vRNP structures during viral RNA synthesis. By virtue of combining these techniques, we unambiguously demonstrated that two different types of vRNP-RNA complexes are produced during RNA synthesis: helical rod-shaped vRNPs with structured RNA and deformed non-helical vRNPs with looped dsRNA. Our results suggest that some vRNPs probably maintain their helical structures for repetitive transcription and/or replication; however, some vRNPs probably fail repetitive RNA synthesis due to deformation of their helical structures.

vRNP synthesizing structured viral RNA was not greatly deformed, and maintained its helical rod-shaped structure (Fig. 1e, f). The helical rod-shaped configuration of vRNP associated with structured RNA was very similar to that of the vRNPs in a static state. However, we presume that these two structures are essentially different. In vRNP in a static state, the RNA polymerase complex exists at the tip of the helical, rod-shaped vRNP, as reported (7–9). However, in vRNP synthesizing structured RNA, localization of the RNA polymerase was likely not limited to the tip of the helical

229 rod-shaped vRNP, since the structured viral RNA was not only associated with the tip,
230 but also with the body of the rod-shaped vRNP (Fig. 1, Supplementary Fig. 3). In support
231 of this observation, Coloma *et al*. recently reported localization of RNA polymerase on
232 the body of the helical rod-shaped vRNP during transcription (31). Although the nascent
233 RNA structures in their cryo-EM images were not well resolved, vRNPs they observed
234 would correspond to vRNPs producing structured RNAs in our observations.

235 Although we could not determine whether structured RNA associated with the
236 helical vRNPs was mRNA or cRNA, the vRNPs with structured RNA are consistent with
237 the progressive helical track transcription model proposed by Coloma *et al* (31).
238 Therefore, we propose that helical vRNPs with structured RNA represent the correct
239 transcription mode, because maintenance of the helical, rod-shaped vRNP structure is
240 favourable to commence the next round of RNA synthesis (Fig. 6). Assuming that the
241 structured RNA is an mRNA, the 5'-terminus of vRNA is associated with RNA
242 polymerase throughout transcription (25, 37). If the 3' end of vRNA was released from
243 RNA polymerase in this process, the helical structure of the vRNP would be largely
244 loosened (Supplementary Fig. 7, pattern A). However, such a loosened vRNP structure
245 has never been observed, suggesting that the 3' end of the vRNA is not detached, which
246 is consistent with a recent finding that the 3' end of vRNA binds to the secondary binding

247 site of RNA polymerase after transcription (18). Therefore, we propose that in
248 transcription, vRNPs maintain the double-helical structure in which both 3' and 5' ends of
249 the vRNA are bound by the RNA polymerase throughout mRNA synthesis
250 (Supplementary Fig. 7, pattern B), which is consistent with a model that Coloma *et al*.
251 recently proposed (31).

252 In contrast, the structure of vRNP associated with the looped RNA was largely
253 deformed into non-helical structures, probably because the vRNA is at least partially
254 detached from the NPs of the vRNP (Fig. 1, 2). For the next round of transcription and/or
255 the next replication cycle, the looped dsRNA should be separated and the template vRNA
256 should rebind to the NPs of the vRNP, so that the deformed vRNP is refolded into its
257 native double-helical structure. Considering these complicated events, it is reasonable to
258 presume that deformed vRNPs associated with looped RNA represent a failure of RNA
259 synthesis (Fig. 6). If deformation of vRNPs sometimes occurs in virus-infected cells,
260 some vRNPs would fail to produce nascent RNAs and the encoded viral proteins, while
261 other vRNPs are successful in transcription and/or replication. Indeed, when influenza
262 viruses are infected at low multiplicity of infection, one or more virus proteins are not
263 expressed in some cells (38, 39). Deformation of vRNPs during transcription and/or
264 replication might be related to such observations.

Interestingly, looped RNAs associated with deformed vRNPs were dsRNAs, which are probably composed of nascent RNA and template vRNA (Fig. 3–5). Although it was previously thought that influenza viruses do not produce dsRNA in infected cells (40, 41), dsRNAs were detected in the nuclei of virus-infected cells (Fig. 4e), suggesting that in some cases dsRNAs can be generated during transcription and replication. Although further analysis is needed, this finding suggests that looped dsRNAs observed in this study may be produced in the nuclei of influenza virus-infected cells.

In conclusion, by combining HS-AFM and cryo-EM, we found two morphologically different vRNPs during viral RNA synthesis. Our results suggest that helical structures are prerequisite for successful repetitive transcription and replication, while deformation of helical structures would represent abortive RNA synthesis. There are still many questions to be resolved. Future investigations will attempt to identify the determinants of looped RNA formation and of structured RNA synthesis, and to clarify whether certain host factors prevent abortive dsRNA formation. Our present findings provide novel insights into viral transcription and replication with strong evidence regarding the composition and mechanism of production of viral RNAs.

Methods

Purification of vRNP

Influenza A virus, A/Puerto Rico/8/34 (H1N1) (PR8), was prepared as previously reported (9). Purified PR8 virions (~5 mg mL^{-1}) were lysed in 50 mM Tris-HCl buffer (pH 8.0) containing 100 mM KCl, 5 mM $MgCl_2$, 1 mM dithiothreitol (DTT), 2% Triton X-100, 5% glycerol, 2% lysolecithin, and 1 U μL^{-1} RNasin Plus RNase inhibitor (Promega) for 1 h at 30°C. The sample was ultracentrifuged through a 30–70% (w/v) glycerol gradient in Tris-NaCl buffer (50 mM Tris-HCl, pH 8.0, 150 mM NaCl) at 45,000 rpm for 3 h at 4°C in a SW55Ti rotor (Beckman). Collected fractions were mixed with 2× Tris-glycine SDS sample buffer (Novex) and then subjected to SDS-PAGE, in which a 4–15% Mini Protean TGX precast gel (Bio-rad) was used.

In vitro RNA synthesis using virion-derived RNPs

Purified vRNP (1–2 mg mL^{-1} for cryo-EM and 0.01 mg mL^{-1} for the other experiments) was incubated in 50 mM Tris-HCl buffer (pH 7.9) containing 5 mM $MgCl_2$, 40 mM KCl, 1 mM DTT, 10 μg mL^{-1} actinomycin D, 1 mM each of ATP, CTP, GTP, and UTP, 1 U μL^{-1} RNasin Plus RNase inhibitor with a primer, 1 mM ApG (Iba). In some experiments, 10 μg mL^{-1} rabbit globin mRNA (Sigma) was used as a primer instead of ApG. The

reaction was performed at 30°C for 15 min (for ApG primer) or 30 min (for globin mRNA primer) unless otherwise noted. For detection of newly synthesized RNA by radioisotope, the same reaction mixture was used with the exception that 0.25 μCi μL^{-1} [α-^{32}P] UTP and 0.05 mM UTP were added. After *in vitro* RNA synthesis, RNA was purified with an RNeasy Mini kit (Qiagen), mixed with equal volume of 2× RNA Loading Dye (New England Biolabs), heated at 90°C for 2 min and immediately chilled on ice. The sample was electrophoresed on 4% polyacrylamide gel containing 7 M urea in 0.5x TBE buffer (Nacalai Tesque) at 120 V for 5 h. The gel was dried at 80°C for 2 h, exposed to an imaging plate (BAS-MS 2025, Fujifilm) for 12–24 h and scanned with a Typhoon 3000 Phosphorimager (GE Healthcare). Labelling of nascent RNA with a nucleotide analogue was also performed in the same reaction mixture using 1 mM 5-bromo-UTP (Br-UTP, Sigma) or 1 mM 5-ethynyl-UTP (EUTP, Abcam) instead of UTP. Inhibition of RNA synthesis was evaluated by adding 0.1–100 μM of 6-fluoro-3-hydroxy-2-pyrazinecarboxamide-4-ribofuranosyl-5'-triphosphate (T-705RTP; kindly provided by Furuta Y., Fujifilm Toyama Chemical Co., Ltd.) to the reaction mixture.

Preparation of viral RNAs with T7 RNA polymerase

RNA standards for NP and NA segments of PR8 virus were prepared as described

317 previously (34). Templates containing a T7 phage promoter sequence
318 (TAATACGACTCACTATAGGG) were amplified by PCR using sets of primers listed in
319 Supplementary Table 1 and pPolI plasmid harbouring the sequence of each segment (42).
320 PCR products were purified with a Min Elute Gel Extraction kit (Qiagen) and were
321 transcribed *in vitro* with RiboMAX Large Scale RNA Production Sysytem-T7 (Promega)
322 according to the supplier's protocol. After RQ1 DNase I (Promega) treatment for 30 min
323 at 37°C, transcripts were purified using an RNeasy Mini kit. The concentration of purified
324 RNA was determined by spectrophotometry and the copy number was calculated from
325 the molecular weight of each RNA. 1×10^{10} copies of RNA were subjected to
326 electrophoresis (a 4% polyacrylamide gel containing 7 M urea) and visualised with silver
327 staining using a Silver Staining II kit (Wako). In addition, all 8 vRNA segments of
328 influenza A virus (A/WSN/33 strain) were similarly prepared and used as markers for
329 electrophoresis. Template DNAs were amplified with the primers listed in Supplementary
330 Table 2 and transcribed by T7 RNA polymerase using 0.25 μCi μL^{-1} [α-^{32}P] UTP.
331 Transcribed RNAs were purified and mixed before electrophoresis.
332
333 **Reverse transcription-quantitative real-time polymerase chain reaction (RT-qPCR)**
334 RT-qPCR was performed according to the protocol of Kawakami *et al*. (34). RNA

335 standard or *in vitro* transcribed virus RNA was mixed with a quarter volume of 10 μM
336 tagged primer (for the sequence see Supplementary Table 3) and incubated at 65°C for 10
337 min. After immediately chilling on ice for 5 min, the mixture was pre-heated at 60°C for
338 5 min. Then 3 volumes of the reaction mixture (final concentration of 1× First Strand
339 buffer (Invitrogen), 5 mM DTT, 0.5 mM each dNTP mix, 10 U μL^{-1} Superscript III
340 reverse transcriptase (Invitrogen), 1 U μL^{-1} RNasin Plus RNase inhibitor: prepared with
341 saturated trehalose and preheated at 60°C for 5 min) were added to the RNA solution at
342 60°C, and the mixture was further incubated for 1 h at 60°C. The reaction was stopped
343 by heating the mixture at 85°C for 5 min, and the cDNA solution was stored on ice until
344 use. Fifty-fold diluted cDNA solution was mixed with forward and reverse qPCR primers
345 (each final 1 μM, for sequences see Supplementary Table 3), and an equal volume of
346 Thunderbird SYBR qPCR mix (Toyobo) was added. The qPCR reaction was performed
347 on Rotor-Gene Q (Qiagen) and the conditions were 95°C for 1 min, followed by 40 cycles
348 of 95°C for 15 sec and 60°C for 30 sec. For absolute quantitation, 10-fold serial dilutions
349 (1×10^9–1×10^4 copies μL^{-1}) of synthetic RNA standards prepared as described above
350 were used to generate a standard curve. The copy number was calculated from the
351 standard curve with a strong linear correlation ($R^2 > 0.99$) and amplification efficiency
352 between 95 and 105%.

353

354 **High-speed atomic force microscopy (HS-AFM)**

355 Samples for HS-AFM imaging were prepared in a microcentrifuge tube, dropped onto
356 freshly cleaved mica without surface modification, and incubated for the desired time
357 (generally 1–5 min) at room temperature. The mica surface was then washed sufficiently
358 with imaging buffer (50 mM Tris-HCl (pH 7.9), 5 mM $MgCl_2$, 40 mM KCl, 1 mM DTT).
359 The sample was observed in the imaging buffer at room temperature using an HS-AFM
360 System (Nano Explorer, RIBM). Images were taken at 2 images s^{-1} using cantilevers with
361 a 0.1 N m^{-1} spring constant and a resonance frequency in water of 0.6 MHz (BL-AC10DS,
362 Olympus). In order to acquire high-resolution images, the electron beam-deposited tips
363 were fabricated using phenol or ferrocene powder, as described in Uchihashi *et al* (43).
364 Incorporation of Br-UTP into nascent RNA was confirmed by incubating *in vitro*
365 transcripts with 0.1 mg mL^{-1} monoclonal anti-5-bromodeoxyuridine antibody
366 (SAB4700630, Sigma) for 2 h at 4°C in a microcentrifuge tube and imaging the sample
367 with HS-AFM. Production of the dsRNA was examined by adding 1 μg mL^{-1} J2 antibody
368 (10010200, Scicons) to the reaction mixture in a microcentrifuge tube, incubating for 2 h
369 at 4°C, and observing it by HS-AFM. *In situ* observation of RNA digestion by each RNase
370 was performed by adding 1/10 volume of the indicated concentration of RNase A

371 (Epicentre) or ShortCut RNase III (New England Biolabs) to the AFM liquid cell during
372 imaging. At least five independent experiments were performed for each RNase. All HS-
373 AFM images were viewed and analysed with Kodec 4.4.7.39 (44). A low-pass filter and
374 a flattening filter were applied to individual images to remove spike noise and to make
375 the xy-plane flat, respectively.
376
377 **Cryo-electron microscopy (Cryo-EM)**
378 One microliter of reaction solution of the vRNP was applied to a glow-discharged holey
379 carbon grid (Quantifoil R1.2/1.3, Cu 300 mesh) and blotted manually, followed by
380 application of 2 μL of reaction solution, blotting and rapid freezing in liquid ethane on a
381 Vitrobot Mark IV (Thermo Fisher Scientific). Images were recorded close to focus with
382 a Volta phase plate on a Talos Arctica electron microscope equipped with a Falcon III
383 camera (Thermo Fisher Scientific) in integrating mode. The total dose during a single
384 exposure was ~40 electrons/$Å^2$.
385 For cryo-electron tomography, 2 μL of reaction solution of the vRNP mixed with colloidal
386 gold (1.9 nm or 5 nm diameter) were applied to glow-discharged holey carbon grids (C-
387 Flat CF-MH-2C, Protochips Inc.) and rapidly frozen in liquid ethane on a Vitrobot Mark
388 IV (Thermo Fisher Scientific). Images were recorded on a Titan Krios electron

389 microscope equipped with a Falcon II camera (Thermo Fisher Scientific). Tilt series were
390 acquired from −60° to 60° with 2° steps using the Leginon System (45). The total dose
391 during a single tilt series was 120 electrons/Å^2. Tilt series data were processed in IMOD
392 (46) by using gold particles as fiducial markers for manual image registration after 2×
393 binning (final voxel size 4.4 Å^3). A tomogram of the entire field of view was reconstructed
394 using SIRT (Simultaneous Iterative Reconstruction Technique). Volumes of interest were
395 extracted from the reconstructed 3D tomogram and visualised with IMOD and AMIRA
396 6.1 (Thermo Fisher Scientific). Consecutive Z-projections were generated using ImageJ
397 (47).
398
399 **Modification of RNA using Click chemistry**
400 A Click-iT RNA Imaging kit was purchased from Invitrogen. After *in vitro* RNA synthesis
401 with EUTP, the sample was deposited on mica and incubated for 3 min at room
402 temperature. The mica surface was washed with imaging buffer and the following
403 reactions were all performed on mica without drying the surface. Imaging buffer on the
404 mica surface was replaced with Click-iT reaction cocktail (Click-iT RNA reaction buffer
405 containing 4 mM $CuSO_4$, 0.02 mg mL^{-1} biotin azide (Thermo Fisher Scientific), and 0.1×
406 Click-iT reaction buffer additive) and incubated for 30 min under light-shielding. The

mica surface was then washed with imaging buffer and the buffer was replaced with 0.1 mg mL^{-1} of streptavidin solution (Jackson ImmunoResearch). After 15 min of incubation at room temperature, the mica surface was washed again with imaging buffer for the HS-AFM observation.

Immunofluorescence assay (IFA)

Vero cells (ATCC CCL-81) were grown in Eagle's minimum essential medium and seeded on 35-mm glass bottom dish (Matsunami Glass) coated with rat collagen I (Corning) one day before infection. Cells were infected with PR8 virus at MOI of 0.1 and incubated for 10 h in minimum essential medium (Gibco) containing 0.3% BSA. Infected cells were fixed in 4% paraformaldehyde (Nacalai Tesque) for 10 min and permeabilized with 0.1% Triton X-100 in PBS for 10 min. Cells were then washed with PBS and blocked with Blocking One (Nacalai Tesque) for 30 min. After blocking, cells were incubated with anti-NP rabbit polyclonal (GTX125989, GeneTex) and anti-dsRNA mouse monoclonal antibody J2 (10010200, Scicons) overnight at 4°C. Cells were washed with PBS and incubated in Alexa Fluoro 488-conjugated anti-mouse antibody (A11001, Thermo Fisher Scientific) and Hoechst 33342 (Thermo Fisher Scientific) for 1 h at 4°C. After incubation, cells were washed with PBS and incubated in Alexa Fluoro 555-conjugated anti-rabbit

antibody (A21248, Thermo Fisher Scientific) for 1 h at room temperature. All antibodies were diluted in PBS with 10% Blocking One. Section images were recorded and deconvolved using DeltaVision Elite system (GE healthcare) with a 60× oil immersion objective on an Olympus IX71 microscope.

Force measurement by HS-AFM

To measure the force applied to the sample surface, two types of HS-AFM images were taken simultaneously: topographic images and amplitude images. By measuring the thermal noise and the InvOLS (inverse optical lever sensitivity) value [nm V^{-1}] of deflection signal of a cantilever, we determined the spring constant (k_c) [pN nm^{-1}] and quality factor (Q_c) of the cantilever as described previously (48). Determined k_c values were in good agreement with nominal values reported by the manufacturer. During observation, the vRNP was destroyed by gradually lowering the set point. Whether the vRNP was destroyed was judged from the apparent change in the height of the vRNP. After imaging, the amplitude value [V] at the frame in which vRNP was destroyed was measured from the amplitude image, and the obtained value was converted into A_{sp} [nm] using the InvOLS value described above. The free cantilever oscillation amplitude A_0 was measured by releasing the cantilever from the sample surface. The average tip-sample

443 interaction force $<F_{ts}>$ was calculated using the following equation, $<F_{ts}> = k_c (A_0^2 -$

444 $A_{sp}^2)^{1/2}/ Q_c$ (49). For preparation of the control vRNP, we treated 0.01 mg mL^{-1} of vRNP

445 with 0.05 μg mL^{-1} of RNase A for 10 min at 37°C. Degradation of the vRNA was

446 confirmed by RT-PCR using primers for detecting the full-length NP segment.

447

448 **References**

449 1. Eisfeld, A.J., Neumann, G. & Kawaoka, Y. At the centre: influenza A virus

450 ribonucleoproteins. *Nat. Rev. Microbiol.* **13,** 28–41 (2015).

451 2. Ortin, J. & Martin-Benito, J. The RNA synthesis machinery of negative-stranded

452 RNA viruses. *Virology* **479–480,** 532–544 (2015).

453 3. te Velthuis, A.J. & Fodor, E. Influenza virus RNA polymerase: insights into the

454 mechanisms of viral RNA synthesis. *Nat. Rev. Microbiol.* **14,** 479–493 (2016).

455 4. Pflug, A., Lukarska, M., Resa-Infante, P., Reich, S. & Cusack, S. Structural

456 insights into RNA synthesis by the influenza virus transcription-replication machine.

457 *Virus Res.* **234,** 103–117 (2017).

458 5. Compans, R.W., Content, J. & Duesberg, P.H. Structure of the ribonucleoprotein

459 of influenza virus. *J. Virol.* **10,** 795–800 (1972).

460 6. Jennings, P.A., Finch, J.T., Winter, G. & Robertson, J.S. Does the higher order

461 structure of the influenza virus ribonucleoprotein guide sequence rearrangements in

462 influenza viral RNA? *Cell* **34,** 619–627 (1983).

463 7. Moeller, A., Kirchdoerfer, R.N., Potter, C.S., Carragher, B. & Wilson, I.A.

464 Organization of the influenza virus replication machinery. *Science* **338,** 1631–1634

465 (2012).

8. Arranz, R. et al. The structure of native influenza virion ribonucleoproteins. *Science* **338,** 1634–1637 (2012).

9. Sugita, Y., Sagara, H., Noda, T. & Kawaoka, Y. Configuration of viral ribonucleoprotein complexes within the influenza A virion. *J. Virol.* **87,** 12879–12884 (2013).

10. Blaas, D., Patzelt, E. & Kuechler, E. Identification of the cap binding protein of influenza virus. *Nucleic Acids Res.* **10,** 4803–4812 (1982).

11. Guilligay, D. et al. The structural basis for cap binding by influenza virus polymerase subunit PB2. *Nat. Struct. Mol. Biol.* **15,** 500–506 (2008).

12. Plotch, S.J., Bouloy, M., Ulmanen, I. & Krug, R.M. A unique cap(m7GpppXm)-dependent influenza virion endonuclease cleaves capped RNAs to generate the primers that initiate viral RNA transcription. *Cell* **23,** 847–858 (1981).

13. Yuan, P. et al. Crystal structure of an avian influenza polymerase PA(N) reveals an endonuclease active site. *Nature* **458,** 909–913 (2009).

14. Dias, A. et al. The cap-snatching endonuclease of influenza virus polymerase resides in the PA subunit. *Nature* **458,** 914–918 (2009).

15. Reich, S. et al. Structural insight into cap-snatching and RNA synthesis by influenza polymerase. *Nature* **516,** 361–366 (2014).

16. Robertson, J.S., Schubert, M. & Lazzarini, R.A. Polyadenylation sites for influenza virus mRNA. *J. Virol.* **38,** 157–163 (1981).

17. Poon, L.L., Pritlove, D.C., Sharps, J. & Brownlee, G.G. The RNA polymerase of influenza virus, bound to the 5' end of virion RNA, acts in cis to polyadenylate mRNA. *J. Virol.* **72,** 8214–8219 (1998).

18. Wandzik, J.M. et al. A structure-based model for the complete transcription cycle of influenza polymerase. *Cell* **181,** 877–893 (2020).

19. Hay, A.J., Skehel, J.J. & McCauley, J. Characterization of influenza virus RNA complete transcripts. *Virology* **116,** 517–522 (1982).

20. Honda, A., Ueda, K., Nagata, K., & Ishihama, A. RNA polymerase of influenza virus: Role of NP in RNA chain elongation. *J. Biochem.* **104,** 1021–1026 (1988).

21. York, A., Hengrung, N., Vreede, F.T., Huiskonen, J.T. & Fodor, E. Isolation and characterization of the positive-sense replicative intermediate of a negative-strand RNA virus. *Proc. Natl. Acad. Sci. USA* **110,** E4238–4245 (2013).

22. Turrell, L., Lyall, J.W., Tiley, L.S., Fodor, E. & Vreede, F.T. The role and assembly mechanism of nucleoprotein in influenza A virus ribonucleoprotein complexes. *Nat. Commun.* **4,** 1591 (2013).

23. Jorba, N., Coloma, R. & Ortin, J. Genetic trans-complementation establishes a

502 new model for influenza virus RNA transcription and replication. *PLoS Pathog.* **5,**
503 e1000462 (2009).
504 24. Fan, H. et al. Structures of influenza A virus RNA polymerase offer insight into
505 viral genome replication. *Nature* **573,** 287–290 (2019).
506 25. Pflug, A., Guilligay, D., Reich, S. & Cusack, S. Structure of influenza A
507 polymerase bound to the viral RNA promoter. *Nature* **516,** 355–360 (2014).
508 26. Hengrung, N. et al. Crystal structure of the RNA-dependent RNA polymerase
509 from influenza C virus. *Nature* **527,** 114–117 (2015).
510 27. Lukarska, M. et al. Structural basis of an essential interaction between influenza
511 polymerase and Pol II CTD. *Nature* **541,** 117–121 (2018).
512 28. Serna Martin, I. et al. A mechanism for the activation of the influenza virus
513 transcriptase. *Mol. Cell* **70,** 1101–1110 (2018).
514 29. Kouba, T., Drncova, P. & Cusack, S. Structural snapshots of actively transcribing
515 influenza polymerase. *Nat. Struct. Mol. Biol.* **26,** 460–470 (2019).
516 30. Peng, Q. et al. Structural insight into RNA synthesis by influenza D polymerase.
517 *Nat. Microbiol.* **4,** 1750–1759 (2019).
518 31. Coloma, R. et al. Structural insights into influenza A virus ribonucleoproteins
519 reveal a processive helical track as transcription mechanism. *Nat. Microbiol.* **5,** 727–734

(2020).

32. Vreede, F.T. & Brownlee, G.G. Influenza virion-derived viral ribonucleoproteins synthesize both mRNA and cRNA in vitro. *J. Virol.* **81,** 2196–2204 (2007).

33. Furuta, Y. et al. Favipiravir (T-705), a novel viral RNA polymerase inhibitor. *Antiviral. Res.* **100,** 446–454 (2013).

34. Kawakami, E. et al. Strand-specific real-time RT-PCR for distinguishing influenza vRNA, cRNA, and mRNA. *J. Virol. Methods* **173,** 1–6 (2011).

35. Ando, T. High-speed atomic force microscopy. *Curr. Opin. Chem. Biol.* **51,** 105–112 (2019).

36. Baudin, F., Bach, C., Cusack, S. & Ruigrok, R.W. Structure of influenza virus RNP. I. Influenza virus nucleoprotein melts secondary structure in panhandle RNA and exposes the bases to the solvent. *EMBO J.* **13,** 3158–3165 (1994).

37. Pritlove, D.C., Poon, L.L., Fodor, E., Sharps, J. & Brownlee, G.G. Polyadenylation of influenza virus mRNA transcribed in vitro from model virion RNA templates: requirement for 5' conserved sequences. *J. Virol.* **72,** 1280–1286 (1998).

38. Martin, K. & Helenius, A. Nuclear transport of influenza virus ribonucleoproteins: the viral matrix protein (M1) promotes export and inhibits import. *Cell* **67,** 117–130 (1991).

538 39. Brooke, C.B. et al. Most influenza a virions fail to express at least one essential
539 viral protein. *J. Virol.* **87,** 3155–3162 (2013).
540 40. Weber, F., Wagner, V., Rasmussen, S.B., Hartmann, R. & Paludan, S.R. Double-
541 stranded RNA is produced by positive-strand RNA viruses and DNA viruses but not in
542 detectable amounts by negative-strand RNA viruses. *J. Virol.* **80,** 5059–5064 (2006).
543 41. Pichlmair, A. et al. RIG-I-mediated antiviral responses to single-stranded RNA
544 bearing 5'-phosphates. *Science* **314,** 997–1001 (2006).
545 42. Neumann, G. et al. Generation of influenza A viruses entirely from cloned
546 cDNAs. *Proc. Natl. Acad. Sci. USA* **96,** 9345–9350 (1999).
547 43. Uchihashi, T., Kodera, N. & Ando, T. Guide to video recording of structure
548 dynamics and dynamic processes of proteins by high-speed atomic force microscopy.
549 *Nat. Protoc.* **7,** 1193–1206 (2012).
550 44. Ngo, K.X., Kodera, N., Katayama, E., Ando, T. & Uyeda, T.Q. Cofilin-induced
551 unidirectional cooperative conformational changes in actin filaments revealed by high-
552 speed atomic force microscopy. *Elife* **4,** e04806 (2015).
553 45. Suloway, C. et al. Automated molecular microscopy: the new Leginon system. *J.*
554 *Struct. Biol.* **151,** 41–60 (2005).
555 46. Kremer, J.R., Mastronarde, D.N. & McIntosh, J.R. Computer visualization of

556 three-dimensional image data using IMOD. *J. Struct. Biol.* **116,** 71–76 (1996).

557 47. Schneider, C.A., Rasband, W.S. & Eliceiri, K.W. NIH Image to ImageJ: 25 years

558 of image analysis. *Nat. Methods* **9,** 671–675 (2012).

559 48. Rico, F., Gonzalez, L., Casuso, I., Puig-Vidal, M. & Scheuring, S. High-speed

560 force spectroscopy unfolds titin at the velocity of molecular dynamics simulations.

561 *Science* **342,** 741–743 (2013).

562 49. Garcia, R. *Amplitude modulation Atomic Force Microscopy* (Wiley, 2010).

563

564

565

Acknowledgements

We thank Yousuke Furuta for providing us with T-705RTP; Yoshihiro Kawaoka for providing us with plasmids; Ichiro Taniguchi, Keiko Shindo, Akiko Makino, and Keizo Tomonaga for technical assistance; Akira Ishihama for helpful discussion; Toshio Ando and Takayuki Uchihashi for technical support and valuable discussions at Bio-AFM Summer School 2014 held at Kanazawa University. We also thank Editage (www.editage.com) for English language editing. We thank Steven D. Aird for technical editing (www.sda-technical-editor.org). This work was supported by a JSPS Grant-in-Aid for Scientific Research (C) (16K08808, 19K07575) (to MN), a JSPS Grant-in-Aid for Early-Career Scientists (19K16667), a Research Grant from the Kazato Research Encouragement Prize (to YS), an AMED Platform project for Supporting Drug Discovery and Life Science Research (BINDS) (JP18am0101076) (to MW), a Japan Science and Technology Agency PRESTO grant (JPMJPR13L9), a JSPS Grant-in-Aid for Scientific Research (B) (17H04082, 20H03494), a JSPS Grant-in-Aid for Challenging Research (Exploratory) (19K22529), JSPS Core-to-Core Program A, a MEXT Grant-in-Aid for Scientific Research on Innovative Area (19H04831), an AMED Research Program on Emerging and Re-emerging Infectious Disease grants (19fk0108113, 20fk0108270h0001), a Grant from the Daiichi Sankyo Foundation of Life Science, and

584 the Uehara Memorial Foundation (to TN), and grants from the Joint Research Project of
585 the Institute of Medical Science, the University of Tokyo, the Joint Usage/Research
586 Center program of Institute for Frontier Life and Medical Sciences Kyoto University, and
587 the Takeda Science Foundation (to YS and TN). MW was supported by direct funding
588 from Okinawa Institute of Science and Technology Graduate University.

589

590 **Author contributions**

591 MN and TN designed the study. MN, YS, NK, SM, and YM performed the experiments.
592 MN, YS, NK, and TN analysed data. MN, YS, MW, and TN wrote the manuscript. All
593 authors reviewed and approved the manuscript.

594

595 **Competing interests**

596 The authors declare no competing interests.

597

598 **Additional information**

599 Supplementary information is available for this paper at https://
600 Correspondence and requests for materials should be addressed to T.N.
601 Reprints and permission information are available at www.nature.com/reprints.

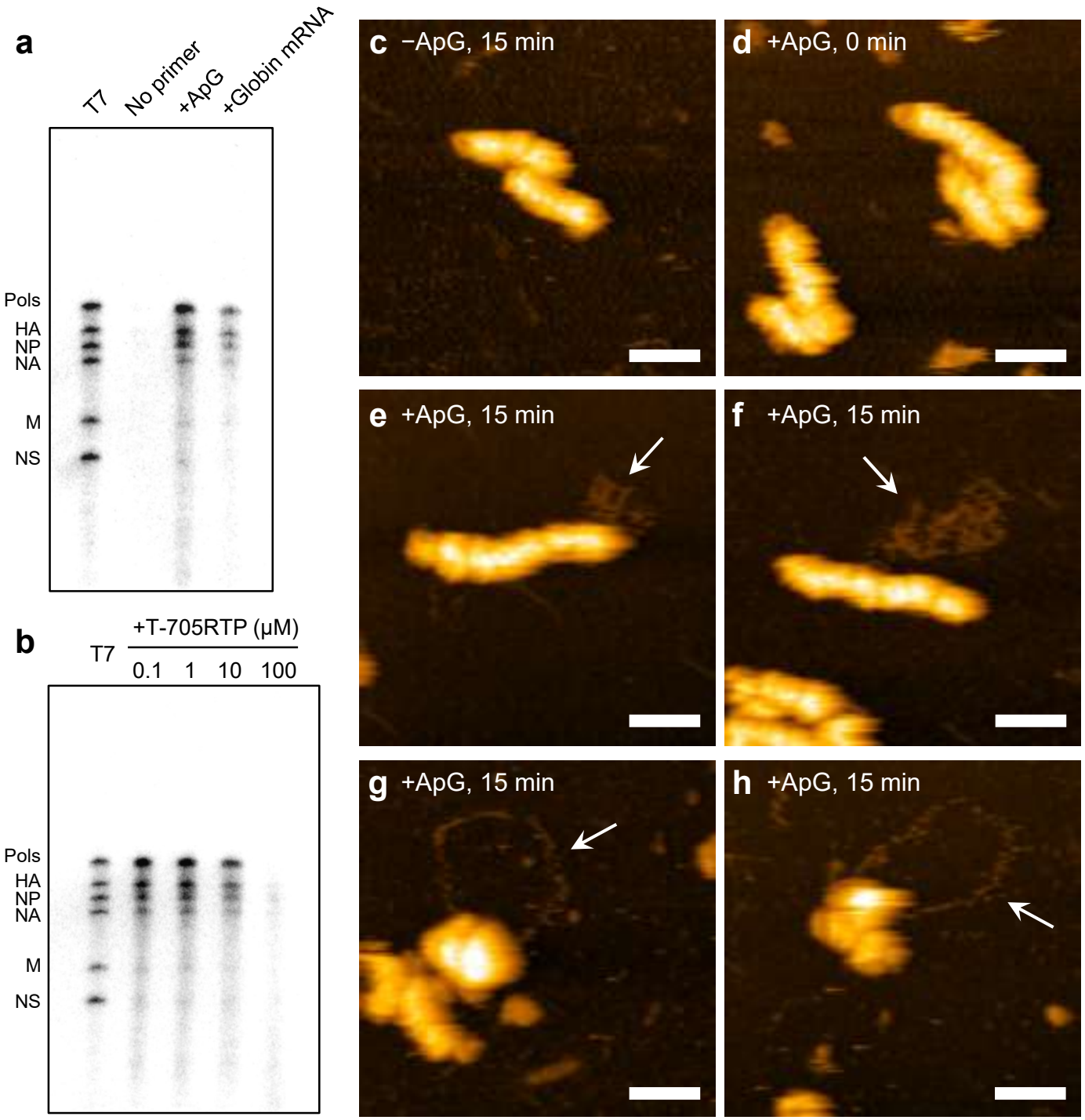

Fig. 1. HS-AFM observation of vRNPs during RNA synthesis.
a, Primer-dependent *in vitro* RNA synthesis using virion-derived vRNPs. RNA was synthesized *in vitro* using ApG or globin mRNA as a primer with 30 min incubation. As a negative control, the reaction mixture was used without primer. A mixture of eight influenza A virus vRNA segments (Pols indicates 3 polymerases, PB2, PB1, and PA) transcribed by T7 RNA polymerase was loaded in the leftmost lane (T7) for evaluation of sizes of the newly synthesized RNAs. **b,** Inhibition of *in vitro* RNA synthesis by T-705RTP. RNA was synthesized *in vitro* using ApG in the presence of the indicated concentration of T-705RTP. All purified RNA samples were analysed on a 4% polyacrylamide gel containing 7 M urea and detected by autoradiography. **c,** As a negative control for the HS-AFM observation, the reaction mixture omitting a primer was used. **d–h,** Virion-derived vRNPs were subjected to *in vitro* RNA synthesis using ApG as a primer. After incubation for 0 min (**d**) or 15 min (**c, e–h**), samples were observed with HS-AFM. Structured and looped RNAs associated with the helical (**e, f**) and deformed vRNPs (**g, h**), respectively, were observed as indicated by arrows at the different positions in the same samples. Scale bars on all images represent 50 nm.

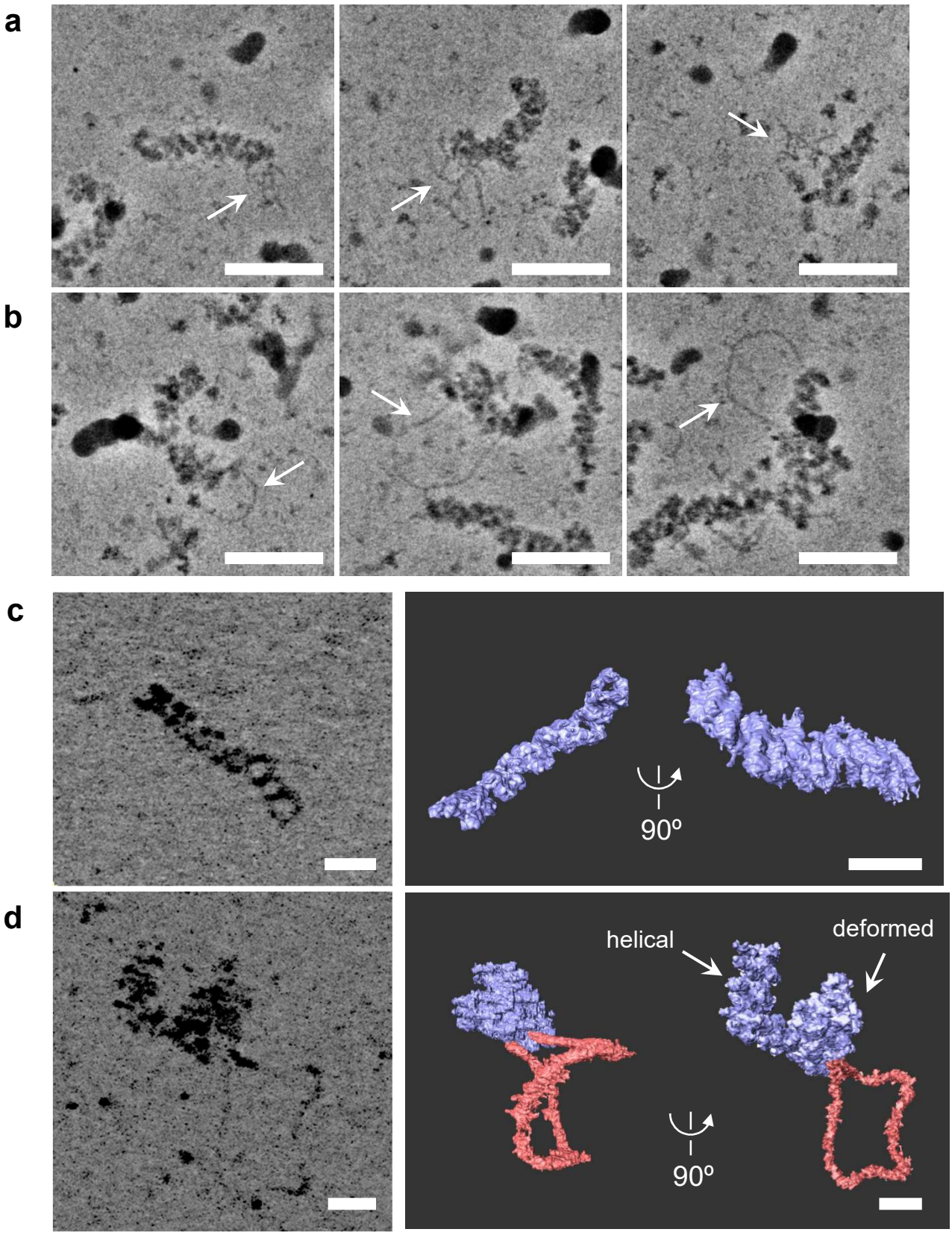

Fig. 2. Cryo-EM observation of vRNPs during RNA synthesis.
An *in vitro* RNA synthesis reaction was performed in the presence of ApG, and was observed with cryo-EM in vitreous ice. Structured RNAs (**a,** arrows) and looped RNAs (**b,** arrows) associated with vRNPs were observed. Scale bars represent 50 nm. (**c, d**) Cryo-ET analysis of vRNPs during RNA synthesis. **c,** Cryo-ET observations of vRNP without RNA synthesis. **d,** Cryo-ET observations of vRNP with RNA synthesis. Left panels: Consecutive Z-projections generated from tomograms; Thickness in Z is 44 nm (**c**) and 88 nm (**d**). Right panels: 3D reconstruction of vRNP segmented from the tomograms. The vRNP and RNA are coloured in blue and red, respectively. Scale bars on all images represent 20 nm.

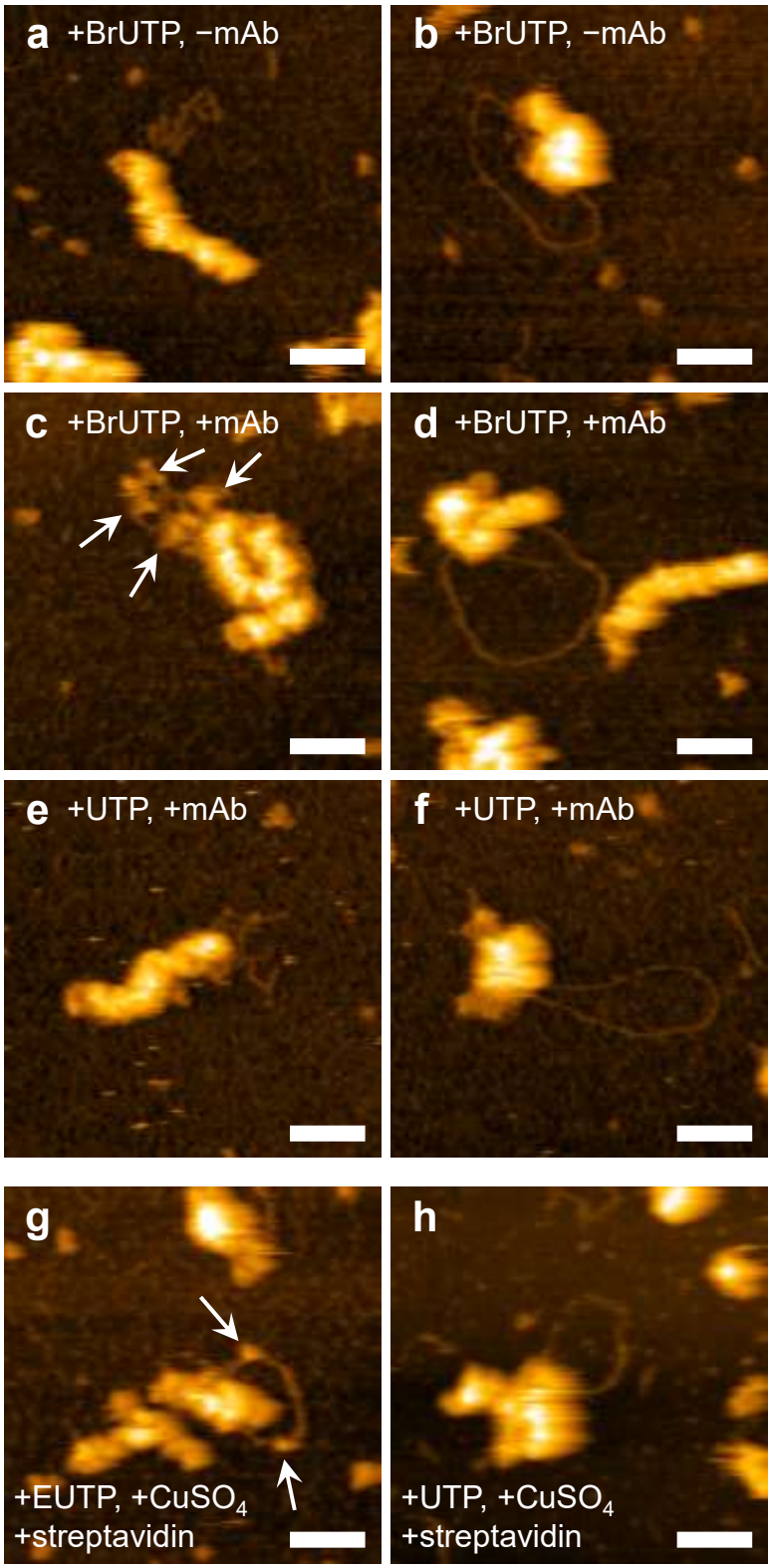

Fig. 3. Incorporation of nucleotide analogues into newly synthesized RNAs.
a-d, Br-UTP was used for *in vitro* RNA synthesis instead of UTP and HS-AFM images were taken without (**a, b**) or with (**c, d**) adding an antibody against Br-UTP. Binding of anti-Br-UTP antibodies was confirmed on structured RNAs (**c,** arrows) while no binding was observed on looped RNAs (**d**). Section analysis of the image (**c**) is shown in Fig. S4. **e, f,** vRNPs were *in vitro* transcribed using UTP and anti-Br-UTP antibody was added to the mixture. **g,** Confirmation of the incorporation of EUTP into looped RNA using Click chemistry. Streptavidin molecules binding to looped RNA are indicated by arrows. **h,** Negative control of the Click reaction. The sample was prepared using UTP instead of EUTP. Each of these results was reproduced at least 3 times. Scale bars, 50 nm.

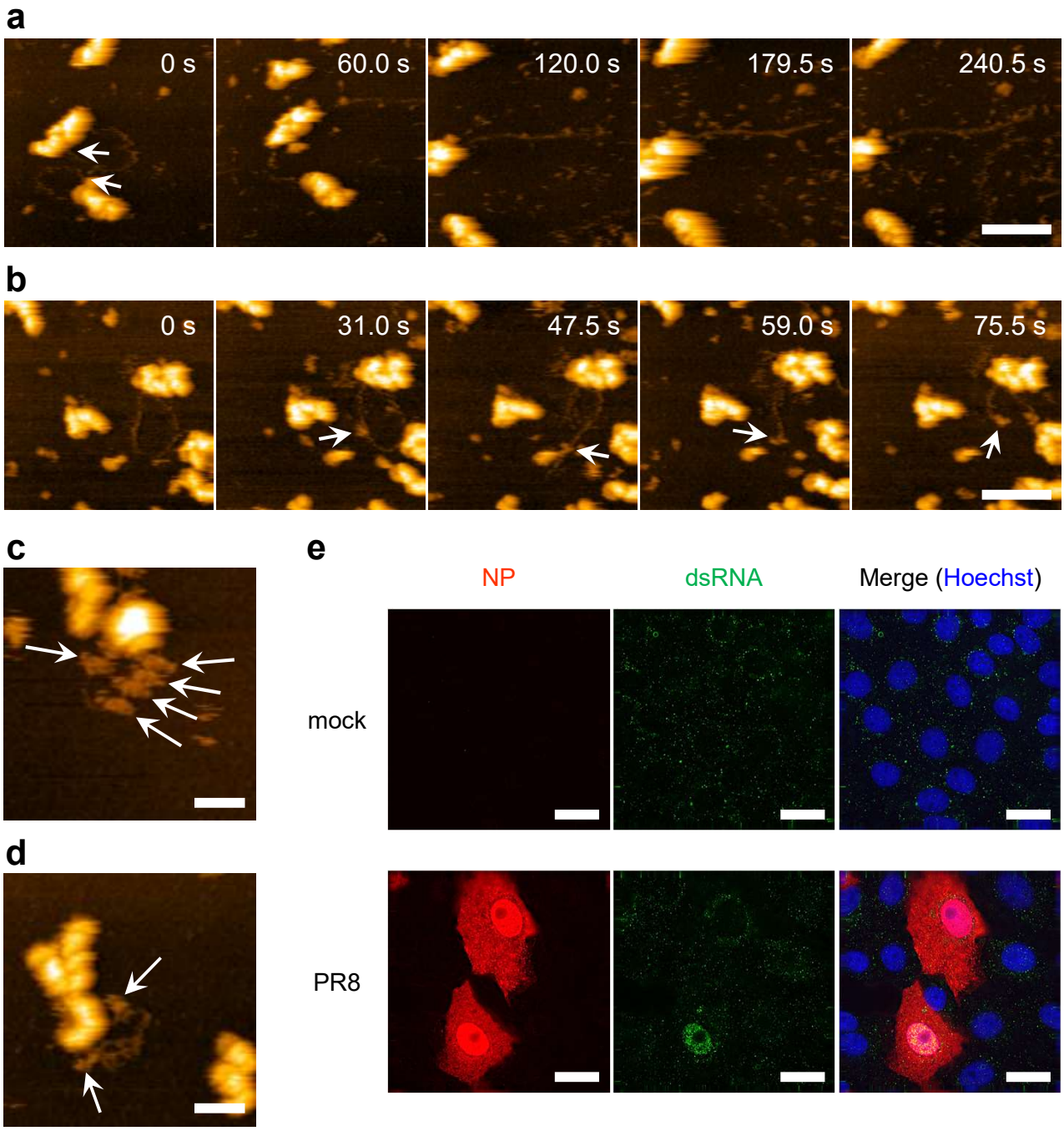

Fig. 4. Production of a double-stranded RNA by vRNP.
a, b, Digestion of looped RNAs with RNases. During HS-AFM observation of looped RNA associated with vRNP, RNase A (**a**) or RNase III (**b**) was added to the liquid chamber at a final concentration of 0.5 μg mL^{-1} or 0.02 U μL^{-1}, respectively. Five images were arbitrarily selected from each movie at the indicated times. One end of the looped RNA was detached from vRNP by adding RNase A at the position indicated by arrows (**a**). By contrast, RNase III digested looped RNA where the RNase bound (**b**, arrows). Scale bars represent 100 nm. **c, d,** Binding of anti-dsRNA antibodies to RNA associated with the vRNP. Antibodies bound to looped RNA (**c**) and to structured RNA (**d**) are indicated by arrows. Results were reproduced at least 5 times. Scale bars in **c, d** represent 50 nm. **e,** Detection of dsRNA in virus-infected cells by IFA. Vero cells were infected with influenza virus PR8 strain at MOI of 0.1. Infected cells were fixed at 10 h post-infection and double-stained with anti-NP and anti-dsRNA antibodies. Cell nuclei were stained with Hoechst. Scale bars, 20 μm.

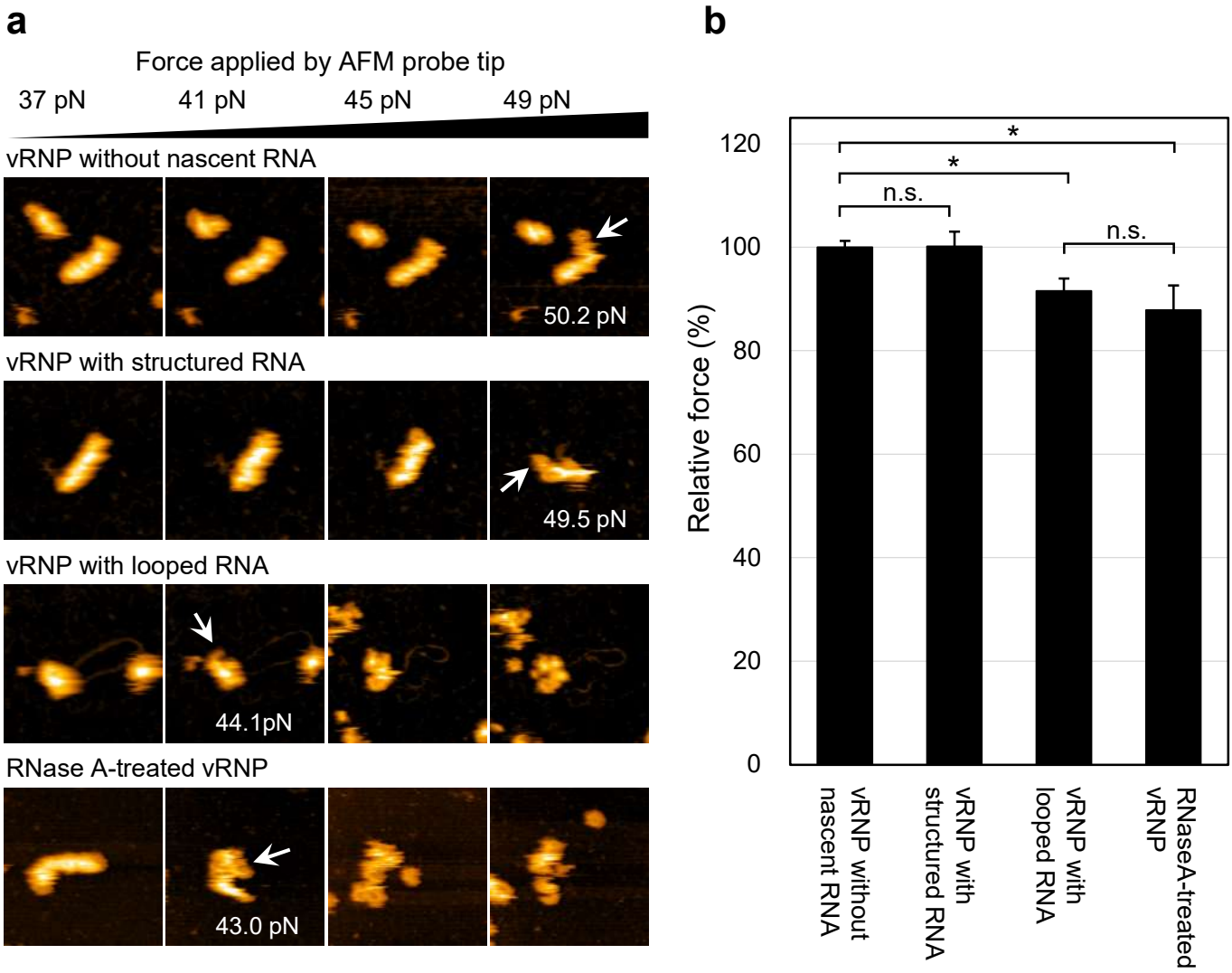

Fig. 5. Deformation of vRNP by releasing the residential vRNA.
a, Deformation of vRNPs with the AFM probe tip. vRNP without a nascent RNA, with a structured RNA or with a looped RNA was deformed by applying force with the cantilever tip during the HS-AFM observation. As a control for the vRNP lacking its intact vRNA, the vRNP pre-treated with RNase A was also deformed. When the vRNP was confirmed as deformed (arrows), the force was measured as described in the Methods. Image sets are representative of 5 vRNPs of each sample and average forces required for deforming vRNPs are calculated. **b,** Structural stability of vRNP during RNA synthesis. The force required for deforming the vRNP without nascent RNA was set as 100% and the relative force of each sample is shown. Significance was determined using the Tukey-Kramer multiple comparison test (*, $P < 0.05$) in R software. Error bars represent the standard deviation of five independent measurements (n.s. = “not significant”).

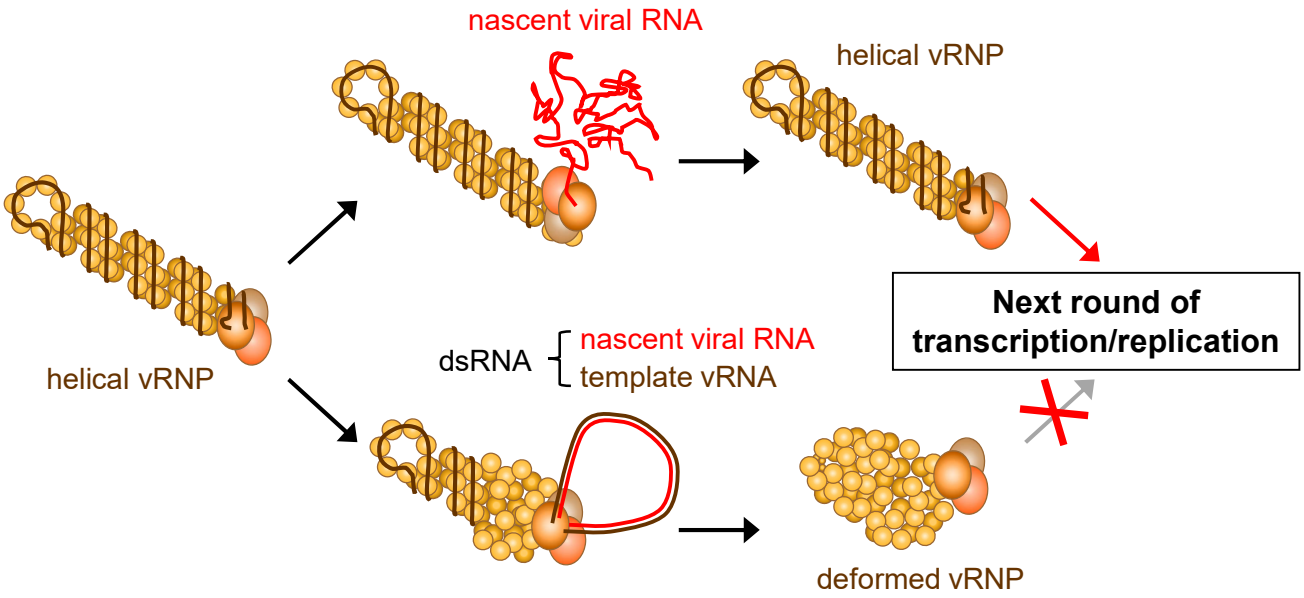

Fig. 6. Model for synthesis of nascent viral RNAs by influenza vRNPs.
When structured viral RNA is synthesized, the vRNP keeps its helical rod-shaped structure and the vRNP is used in next round of transcription and/or replication (upper). In contrast, when looped dsRNA is produced, the vRNP disrupts its helical rod-shaped structure because it loses the residential vRNA. As a result, such deformed vRNP cannot proceed to the next round of transcription and/or replication cycle (lower).

Figures

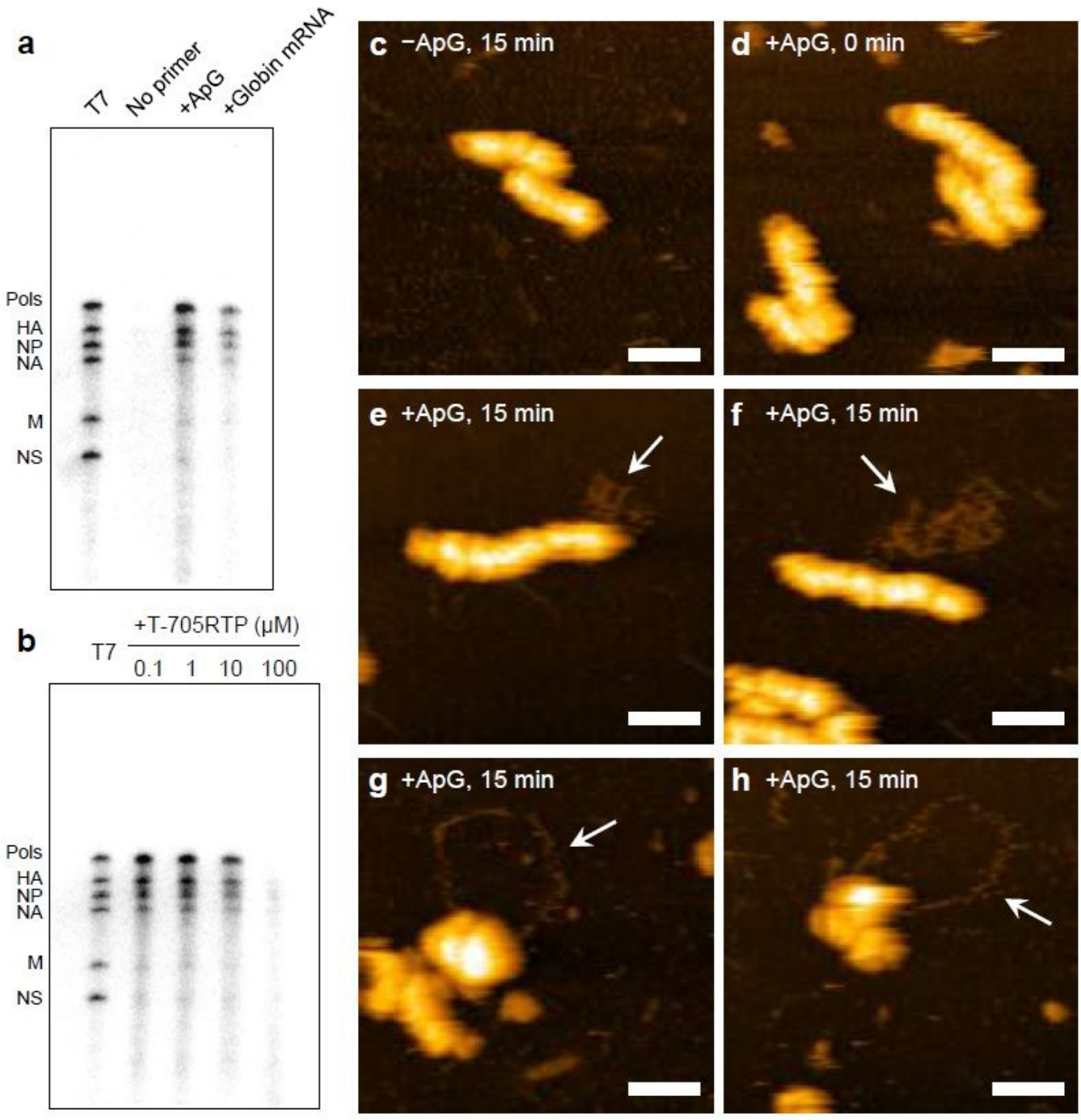

Figure 1

HS-AFM observation of vRNPs during RNA synthesis. a, Primer-dependent in vitro RNA synthesis using virion-derived vRNPs. RNA was synthesized in vitro using ApG or globin mRNA as a primer with 30 min incubation. As a negative control, the reaction mixture was used without primer. A mixture of eight

influenza A virus vRNA segments (Pols indicates 3 polymerases, PB2, PB1, and PA) transcribed by T7 RNA polymerase was loaded in the leftmost lane (T7) for evaluation of sizes of the newly synthesized RNAs. b, Inhibition of in vitro RNA synthesis by T-705RTP. RNA was synthesized in vitro using ApG in the presence of the indicated concentration of T-705RTP. All purified RNA samples were analysed on a 4% polyacrylamide gel containing 7 M urea and detected by autoradiography. c, As a negative control for the HS-AFM observation, the reaction mixture omitting a primer was used. d–h, Virion-derived vRNPs were subjected to in vitro RNA synthesis using ApG as a primer. After incubation for 0 min (d) or 15 min (c, e–h), deformed vRNPs (g, h), respectively, were observed as indicated by arrows at the different positions in the same samples. Scale bars on all images represent 50 nm.

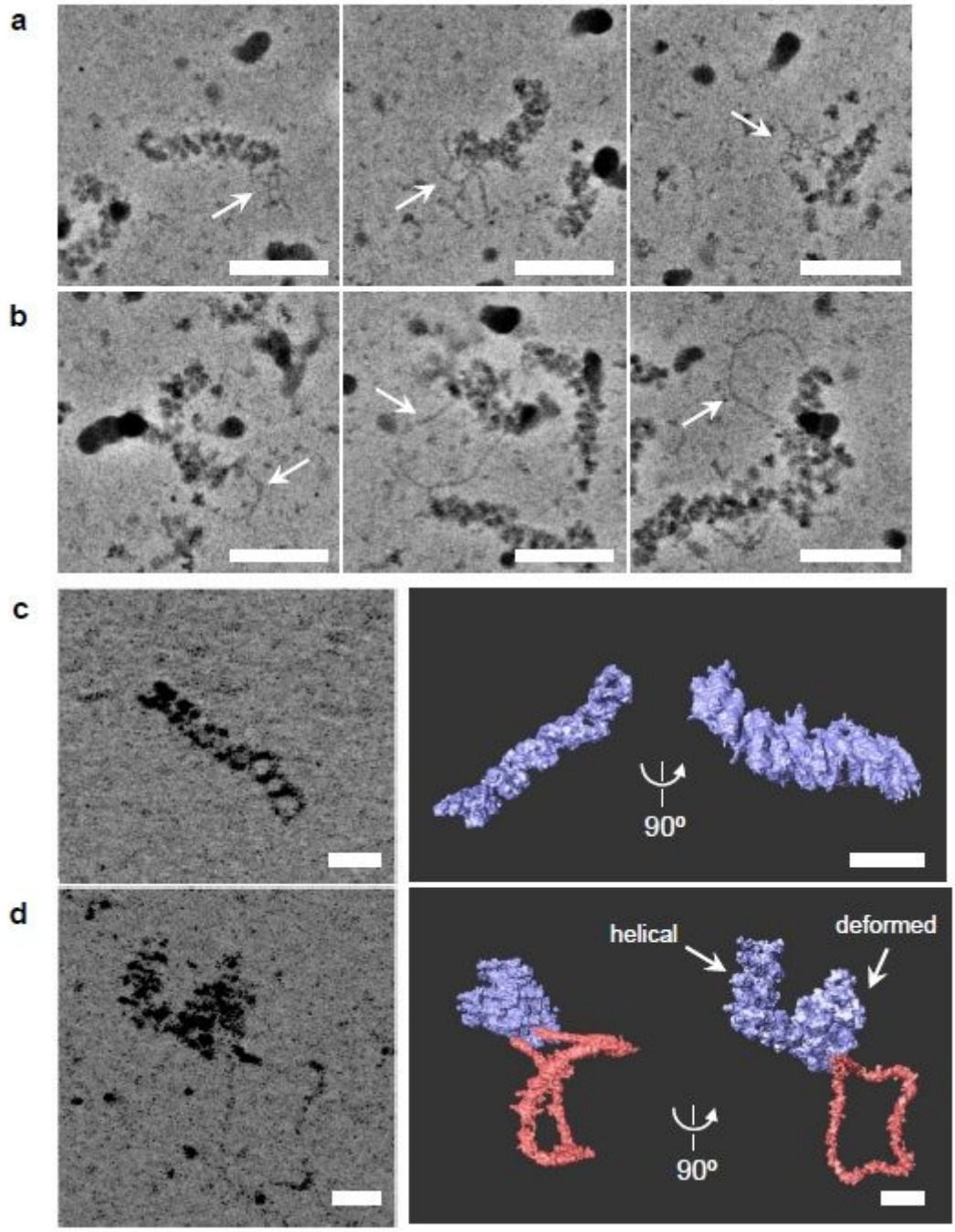

Figure 2

Cryo-EM observation of vRNPs during RNA synthesis. An in vitro RNA synthesis reaction was performed in the presence of ApG, and was observed with cryo-EM in Scale bars represent 50 nm. (c, d) Cryo-ET analysis of vRNPs during RNA synthesis. c, Cryo-ET observations of vRNP without RNA synthesis. d, Cryo-ET observations of vRNP with RNA synthesis. Left panels: Consecutive Z-projections generated from tomograms; Thickness in Z is 44 nm (c) and 88 nm (d). Right panels: 3D reconstruction of vRNP segmented from the tomograms. The vRNP and RNA are coloured in blue and red, respectively. Scale bars on all images represent 20 nm.

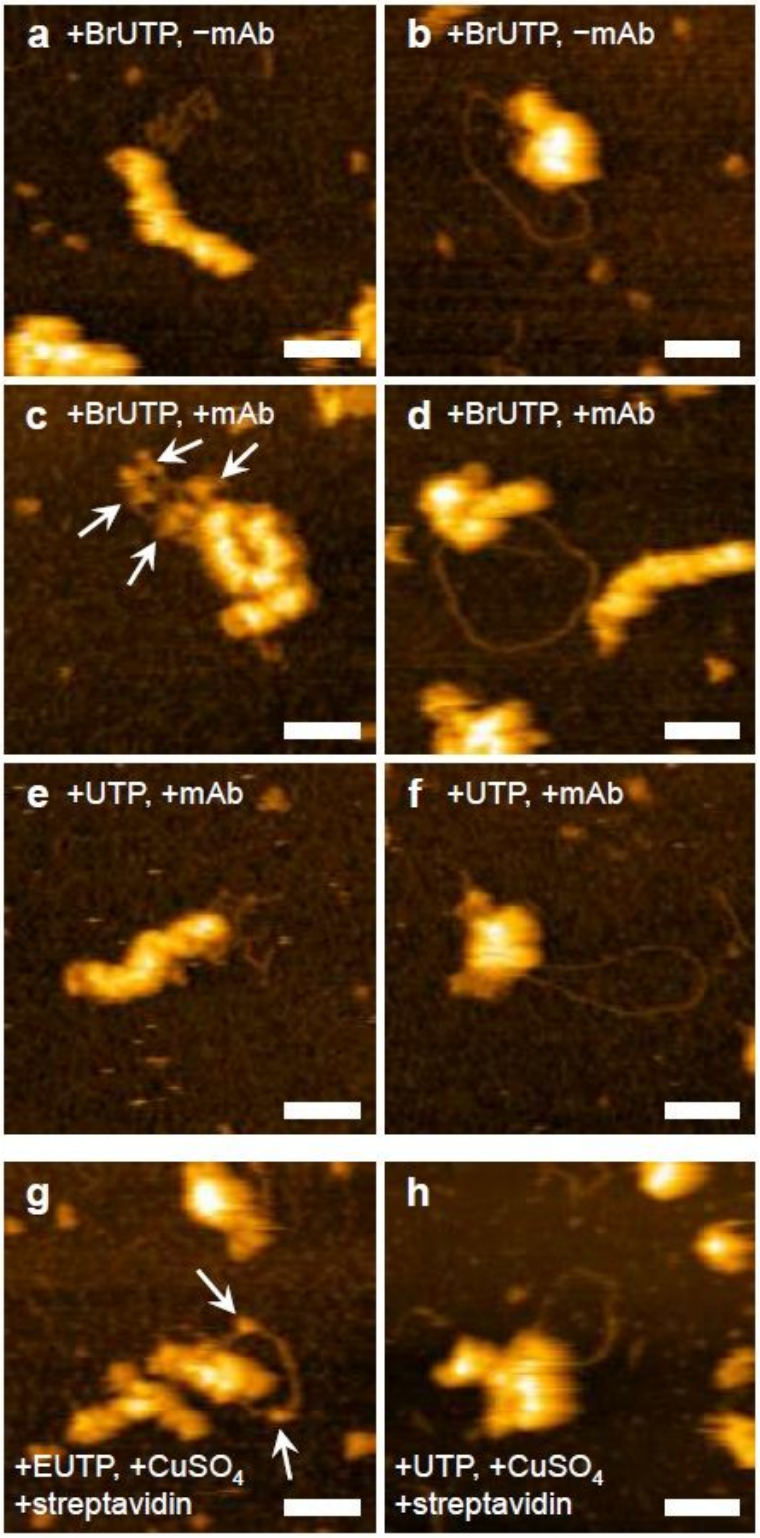

Figure 3

Incorporation of nucleotide analogues into newly synthesized RNAs. a-d, Br-UTP was used for in vitro RNA synthesis instead of UTP and HS-AFM images were taken without (a, b) or with (c, d) adding an antibody against Br-UTP. Binding of anti-Br-UTP antibodies was confirmed on structured RNAs (c, arrows) while no binding was observed on looped RNAs (d). Section analysis of the image (c) is shown in Fig. S4. e, f, vRNPs were in vitro transcribed using UTP and anti-Br-UTP antibody was added to the mixture. g, Confirmation of the incorporation of EUTP into looped RNA using Click chemistry. Streptavidin molecules binding to looped RNA are indicated by arrows. h, Negative control of the Click reaction. The sample was prepared using UTP instead of EUTP. Each of these results was reproduced at least 3 times. Scale bars, 50 nm.

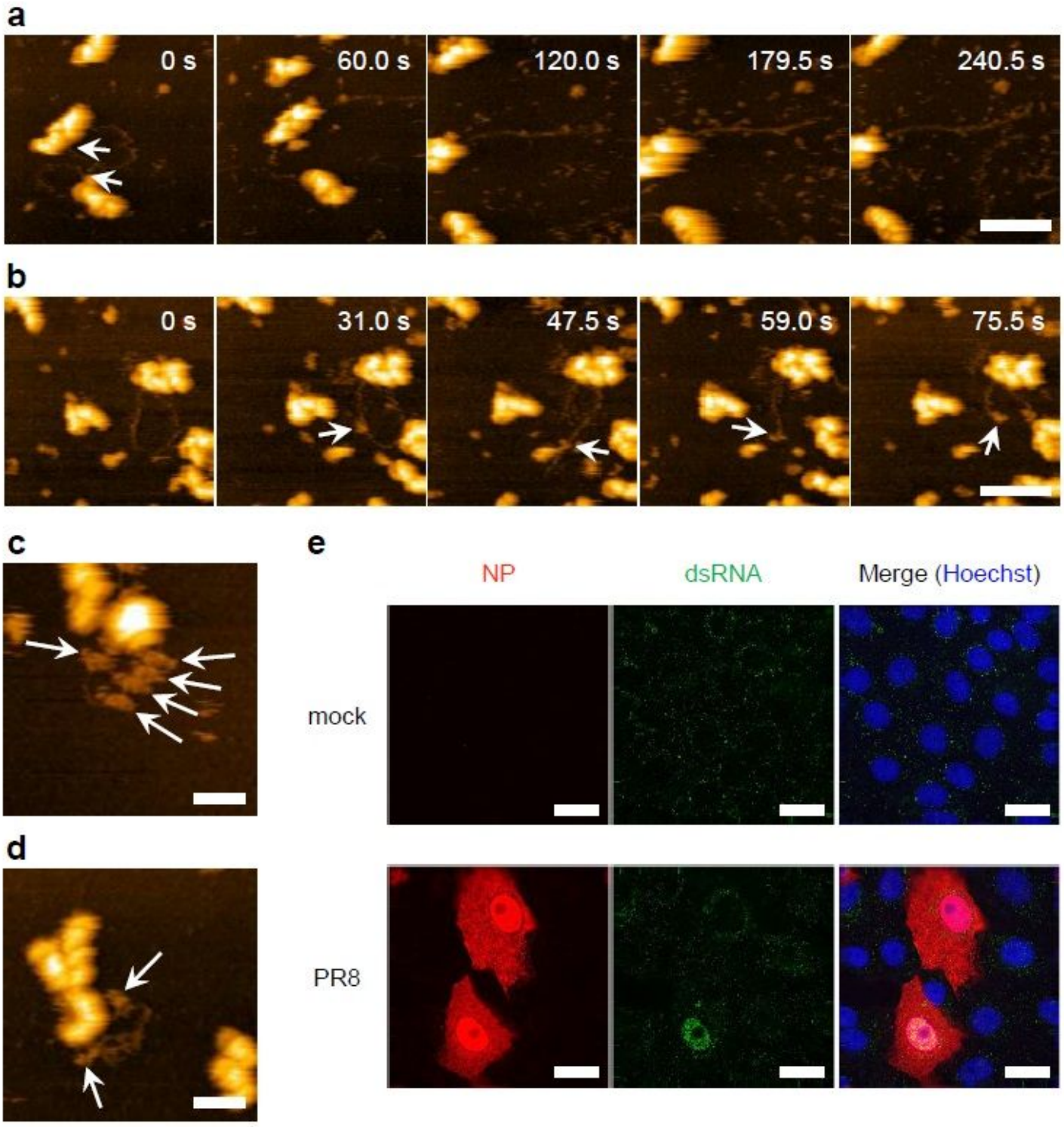

Figure 4

Production of a double-stranded RNA by vRNP. a, b, Digestion of looped RNAs with RNases. During HS-AFM observation of looped RNA associated with vRNP, RNase A (a) or RNase III (b) was added to the liquid chamber at a final concentration of 0.5 μg mL−1 or 0.02 U μL−1, respectively. Five images were arbitrarily selected from each movie at the indicated times. One end of the looped RNA was detached from vRNP by adding RNase A at the position indicated by arrows (a). By contrast, RNase III digested

looped RNA where the RNase bound (b, arrows). Scale bars represent 100 nm. c, d, Binding of anti-dsRNA antibodies to RNA associated with the vRNP. Antibodies bound to looped RNA (c) and to structured RNA (d) are indicated by arrows. Results were reproduced at least 5 times. Scale bars in c, d represent 50 nm. e, Detection of dsRNA in virus-infected cells by IFA. Vero cells were infected with influenza virus PR8 strain at MOI of 0.1. Infected cells were fixed at 10 h post-infection and double-stained with anti-NP and anti-dsRNA antibodies. Cell nuclei were stained with Hoechst. Scale bars, 20 μm.

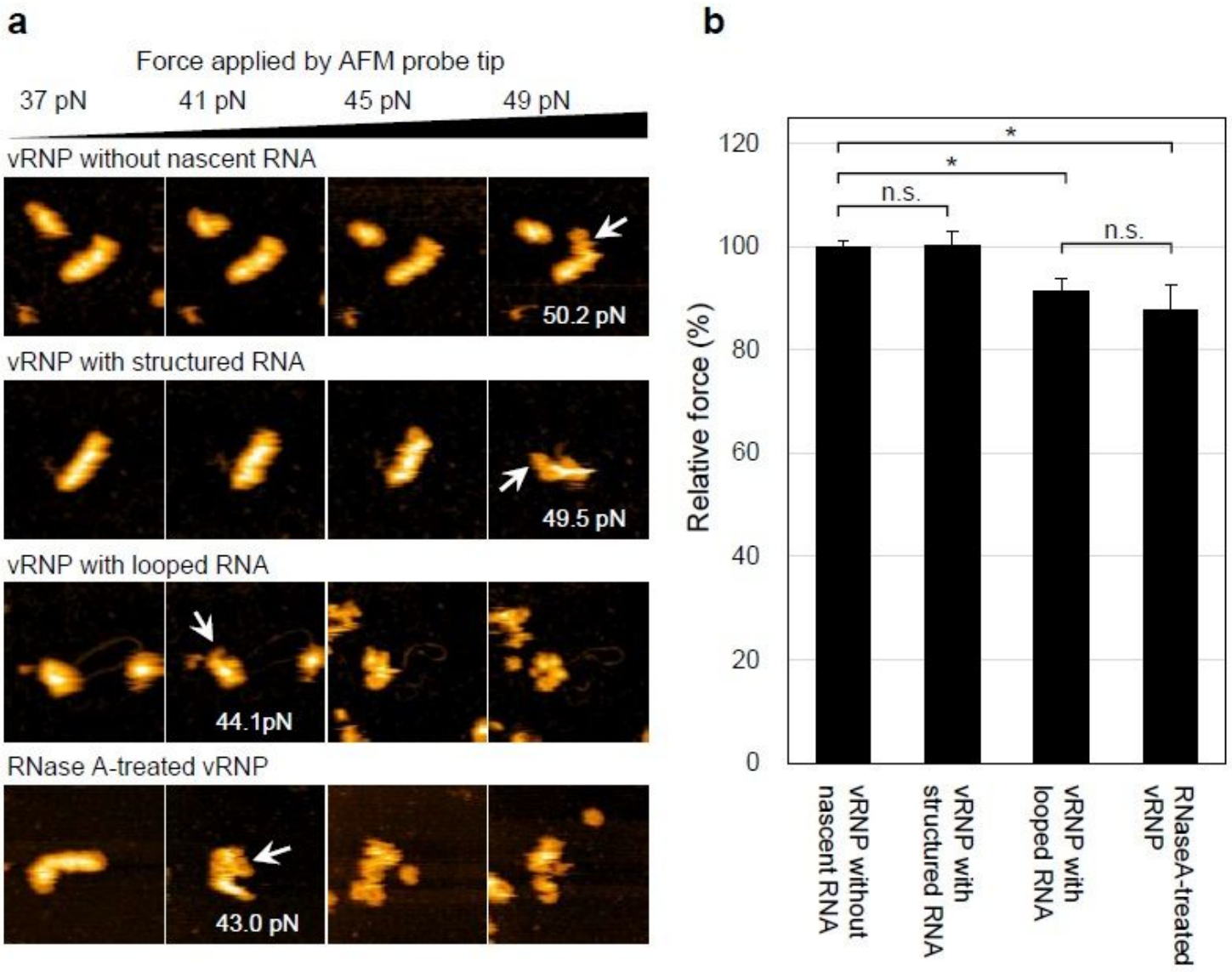

Figure 5

Deformation of vRNP by releasing the residential vRNA. a, Deformation of vRNPs with the AFM probe tip. vRNP without a nascent RNA, with a structured RNA or with a looped RNA was deformed by applying force with the cantilever tip during the HS-AFM observation. As a control for the vRNP lacking its intact vRNA, the vRNP pre-treated with RNase A was also deformed. When the vRNP was confirmed as deformed (arrows), the force was measured as described in the Methods. Image sets are representative of 5 vRNPs of each sample and average forces required for deforming vRNPs are calculated. b, Structural stability of vRNP during RNA synthesis. The force required for deforming the vRNP without nascent RNA

was set as 100% and the relative force of each sample is shown. Significance was determined using the Tukey-Kramer multiple comparison test (*, P < 0.05) in R software. Error bars represent the standard deviation of five independent measurements (n.s. = “not significant”).

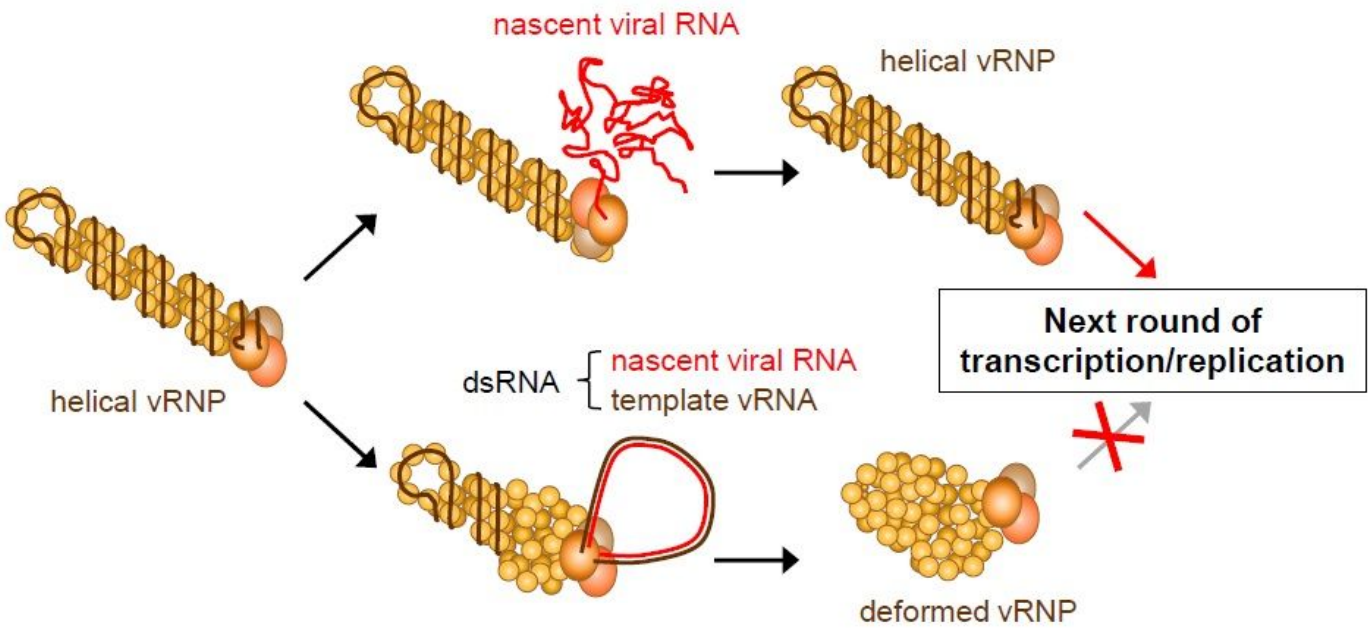

Figure 6

Model for synthesis of nascent viral RNAs by influenza vRNPs. When structured viral RNA is synthesized, the vRNP keeps its helical rod-shaped structure and the vRNP is used in next round of transcription and/or replication (upper). In contrast, when looped dsRNA is produced, the vRNP disrupts its helical rod-shaped structure because it loses the residential vRNA. As a result, such deformed vRNP cannot proceed to the next round of transcription and/or replication cycle (lower).

Supplementary Files

This is a list of supplementary files associated with this preprint. Click to download.

- Supplementarymovie1.mp4
- Supplementarymovie2.mp4
- Supplementarymovie3.mp4
- Supplementarymovie4.mp4
- 210202NakanoSupplementalInformationCommunBiolXXXXXXXXX.pdf